RSC Advances

PAPER

View Article Online
View Journal | View Issue

Cite this: *RSC Adv.*, 2023, **13**, 31541

A facile synthesis of a novel 4-hydroxyl-3-azo coumarin based colorimetric probes for detecting Hg^{2+} and a fluorescence turn-off response of 3CBD to Fe^{3+} in aqueous environment†

Simeon Hamukoshi, *[a] Neliswa Mama,[a] Stiaan Schoeman[a] and Veikko Uahengo [b]

Two azo dyes, (*E*)-3-(benzo[*d*]thiazol-2-yldiazenyl)-4-hydroxy-2*H*-chromen-2-one (**3CBD**) and (*E*)-4-hydroxy-3-(quinolin-2-yldiazenyl)-2*H*-chromen-2-one (**3CQD**), were designed and synthesized using facile methods. The structures were validated through FTIR and NMR spectroscopy. The photophysical property analyses were further studied using UV-Vis and fluorescence spectrophotometers. Consequently, the absorption and emission spectra of **3CBD** confirmed its selectivity of Hg^{2+} and turn-off response to Fe^{3+}. On the other hand, the absorption spectra analysis of **3CQD** demonstrated selectivity in the presence of Hg^{2+}. The colorimetric investigations demonstrated a significant visual response specifically for Hg^{2+}, enabling real-time analysis in the corresponding solutions. The presence of other coexisting metal ions does not interfere with the detection of the target metal ion. The fluorescence studies of the two probes revealed that **3CBD** was highly fluorescent, which was significantly quenched by Fe^{3+}, upon excitation at 340 nm. Utilizing Job plot analyses, it was determined that the complexes **3CBD**–Hg^{2+} and **3CQD**–Hg^{2+} exhibit a binding stoichiometry of 1 : 1. The association constants for these complexes were measured to be 7.48×10^5 and 9.12×10^5 M^{-1}, respectively, indicating a strong association between both probes and their respective metal ions. Both chemosensors exhibited comparable limits of detection (LOD) and limits of quantification (LOQ) of 0.03 μM and 0.10 μM, respectively. Reversible studies confirmed that only chemosensor **3CQD** could serve as a secondary sensor for EDTA. The theoretical studies calculated using Density Functional Theory (DFT) program at B3LYP/6-31G** (Spartan '10 package) level.

Received 15th June 2023
Accepted 23rd October 2023

DOI: 10.1039/d3ra04047j

rsc.li/rsc-advances

1. Introduction

Chemosensing techniques have been gaining momentum in the last few decades in the field of analytical chemistry, due to their simplicity and practicality in applications.[1–4] The increase in human population density over past decades, triggered the technological advancement in many fields of science, to respond to basic needs essential for survival.[5,6] Consequently, these technological advancements come at the cost of environmental pollution, which leads to new diseases and many other implications in the ecosystem.[6–10] Industrial revolutions have been at the center of environmental pollution, especially in the areas such as agriculture for synthetic fertilizers[9,11,12] and pesticides,[8,13,14] food technology,[15–17] film industries[9,18–20] and many others.[6,9,21,22] In essence, the ever-increasing presence of dissolved cations and anions in environmental streams, has become the main source of primary consumption of toxic substances. The presence of dissolved substances in environmental stream have become a serious concern with regard to health hazards, raising concerns even on United Nation agendas, the sustainable development goals.[23] Heavy metals in particular, have been the primary concerns, due to their adverse effects on the ecosystem, mostly on human wellbeing, once their concentration is above threshold.[21,24,25] Moreover, heavy metals such as dissolved elemental mercury are some of the most toxic cations to human physiological systems, with effects which can lead to sudden deaths.[26,27]

Furthermore, mercury(II) ion, a heavy metal, poses significant environmental toxicity,[28,29] even at low concentrations, mercury(II) can cause severe harm to both animals and the human body, usually leading to damage to vital organs like the brain and the potential development of chronic diseases, ultimately resulting in death. Mercury(II) enters the environment through various means, including municipal and industrial wastes, mining activities, battery usage, and fuel

[a]*Department of Chemistry, Faculty of Science, Nelson Mandela University, Port Elizabeth, South Africa. E-mail: vuahengo@unam.na; vuahengo@gmail.com; Tel: +264 61 206 3465*

[b]*Department of Physics, Chemistry and Materials Science, Faculty of Agriculture, Engineering and Natural Sciences, University of Namibia, Windhoek, Namibia*

† Electronic supplementary information (ESI) available. See DOI: https://doi.org/10.1039/d3ra04047j

combustion.[30] Given the evident threat mercury poses to the environment, its ongoing monitoring, control, and detection remain crucial areas of focus.[4,28] Based on these considerations, the development of highly sensitive and selective colorimetric sensors for mercury(II) has gained significant attention. These sensors offer advantages such as simplicity, cost-effectiveness, and ease of operation compared to conventional elemental analytical techniques like Atomic Absorption Spectroscopy (AAS) and Inductive Coupled Plasma-Mass Spectroscopy (ICP-MS).[31–33]

Notably, chemosensing probes that are capable of selectively discriminating target analytes in aqueous solution are highly on demand. To date, a few aqueous based sensing probes have been reported in literature, however, most are haunted by cross-detection problem.[34–37] Thus, the detection of heavy metal cations in aqueous environments are still high on the priority list, due to their prospective of developing field-based sensing kits,[14,38–41] which can be readily used anywhere, including rural areas. In addition, aqueous solution-based sensing probes can be essential in physiological systems, for monitoring the presence and concentration of specific cations of concern, and be able to regulate them. The mode of cation detection is largely based on the design of the molecular framework, normally *via* several interaction mechanisms,[8,42–45] which in many cases characterized by functional groups[46–50] and coordination interaction.[51–54]

Commonly used binding units in colorimetric chemosensors include bipyridines, Schiff bases, guanidine, rhodamine dyes, and azo dyes.[55–57] Among these, azo dyes have gained prominence due to their straightforward synthesis, distinctive photophysical properties, and strong affinity for various heavy metal ions.[58–60] In this study, we present the synthesis of two novel coumarin-based azo probes, namely (*E*)-3-(benzo[*d*]thiazol-2-yldiazenyl)-4-hydroxy-2*H*-chromen-2-one (**3CBD**) which exhibits selectivity for Hg^{2+} under UV-Vis and Fe^{3+} in fluorescence, and (*E*)-4-hydroxy-3-(quinolin-2-yldiazenyl)-2*H*-chromen-2-one (**3CQD**) which specifically detects Hg^{2+} in UV-Vis, both in aqueous solutions.

2. Experiment

2.1 Materials

All reagents and solvents employed for the synthesis of the chemosensors were procured from Sigma Aldrich and Merck and utilized without further purification. Metal solutions of 0.01 M were prepared from nitrates salts (Ag^{+}, Na^{+}, Al^{3+}, Ca^{2+}, Ba^{2+}, Fe^{2+}, Fe^{3+}, Cr^{3+}, Hg^{2+}, Cu^{2+}, Co^{2+}, Cd^{2+}, Zn^{2+}, Li^{+}, Pb^{2+} and Ni^{2+}). UV-Vis and emission spectroscopy measurements were carried out using a PerkinElmer Lambda 35 UV-Vis spectrometer and a PerkinElmer LS 45 fluorescent spectrometer. The spectroscopic analyses were performed in a standard 3.0 ml quartz cuvette with a path length of 1 cm. Fourier Transform Infrared (FT-IR) data was collected using a PerkinElmer FT-IR 180 spectrometer, employing KBr discs. Proton Nuclear Magnetic Resonance (^{1}H NMR) and Carbon-13 Nuclear Magnetic Resonance (^{13}C NMR) analyses were conducted on a Bruker Advance DPX 400 Spectrometer operating at 400 MHz. The NMR experiments were carried out in $CDCl_3$ and d_6-DMSO solvents at room temperature, with tetramethyl silane (TMS) serving as the internal reference.

2.2 Synthesis and characterization 3BD and 3QD

The chemosensors **3CBD** and **3CQD** were synthesized in a one-step reaction according to Scheme 1. The procedure involved the dropwise addition of their respective diazonium salt solutions (0.01 mol) to a coupling 4-hydroxy coumarin solution (0.01 mol) in a methanol/water mixture (30 ml) under ice conditions for 0.5 h with continuous stirring. The products were obtained after the addition of concentrated ammonia solution,[61–64] filtered, and recrystallized in ethanol to yield a brown **3CBD**

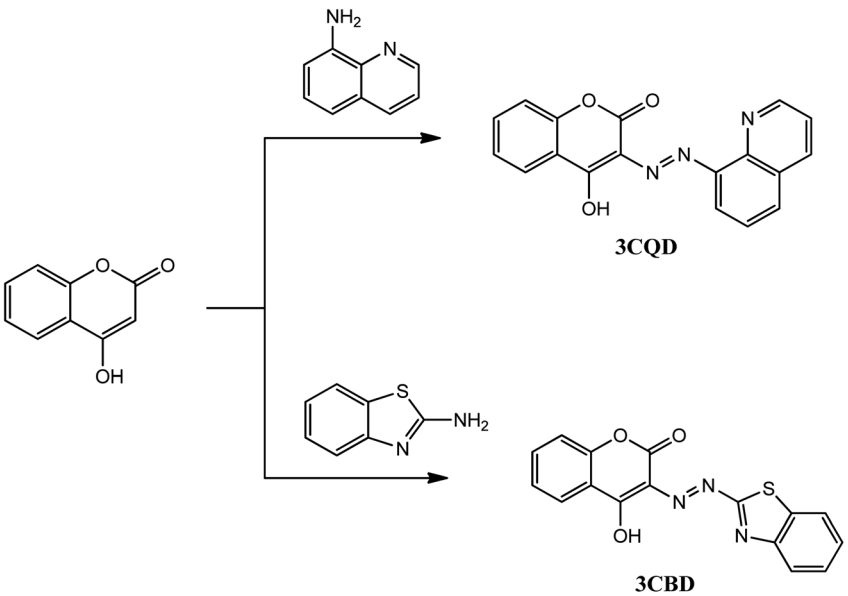

Scheme 1 Reaction scheme of 3CQD and 3CBD.

precipitate and an orange **3CQD** precipitate. The orange solid of **3CBD** was obtained in a yield of 92%. Its FT-IR ν_{max} (cm^{-1}) was found to be 3393 (O–H), 3302 (≡C–H), 1683 (C=O), and 1601 (C=C) (Fig. S4†). The ^1H NMR ($CDCl_3$, 400 MHz) showed peaks at δ = 15.53 (s, OH), 9.11 (d, J = 8.46 Hz, 1H), 8.29 (d, J = 8.84, 1H), 8.24 (d, 1H), 7.84 (d, 1H), 7.73 (d, 1H), 7.69 (d, 1H), 7.38 (d, 1H), and 7.32 (d, 1H) (Fig. S1 and S3†). The brown solid of **3CQD** was obtained in a yield of 92%. Its FT-IR ν_{max} (cm^{-1}) was found to be 3393 (O–H), 3302 (≡C–H), 1683 (C=O), and 1601 (C=C) (Fig. S5†). The ^1H NMR ($CDCl_3$, 400 MHz) showed peaks at δ = 15.53 (s, OH), 9.11 (d, J = 8.46 Hz, 1H), 8.29 (d, J = 8.84, 1H), 8.24 (d, 1H), 7.84 (d, 1H), 7.73 (d, 1H), 7.69 (d, 1H), 7.38 (d, 1H), and 7.32 (d, 1H) (Fig. S1 and S2†).

3. Results and discussions

3.1 Effect of metal ions on photophysical properties of 3CBD and 3CQD

3.1.1. UV vis absorption assay: metal screening/selectivity. The binding affinity of both **3CQD** and **3CBD** towards various cations, including Ag^+, Na^+, Al^{3+}, Ca^{2+}, Ba^{2+}, Fe^{2+}, Fe^{3+}, Cr^{3+}, Hg^{2+}, Cu^{2+}, Co^{2+}, Cd^{2+}, Zn^{2+}, Li^+, Pb^{2+}, and Ni^{2+}, was investigated using UV-Vis spectroscopy. In its unbound state, **3CQD** exhibited an absorption band at 450 nm in an aqueous ethanol solution, and significant spectral changes were observed upon the addition of 0.5 molar equivalents of Hg^{2+} and Co^{2+} (Fig. 1A). The incremental addition of Hg^{2+} to the **3CQD** solution led to a decrease in the absorption band at 450 nm and the appearance of two peaks at 397 nm and 506 nm (Fig. 1B). This was accompanied by a noticeable colour change from yellow to pink. However, no spectral or colour changes were observed when aliquots of Co^{2+} were added to **3CQD** (Fig. 2).

In the case of **3CBD**, its spectral pattern exhibited an absorption band at 464 nm in an aqueous acetonitrile solution. Upon the addition of 1 molar equivalence of Fe^{2+}, Cu^{2+}, and Hg^{2+}, new absorbance peaks were observed at 464 nm, 468 nm, and 537 nm, respectively (Fig. 3A). The gradual addition of Hg^{2+} to the **3CBD** solution led to the actual formation of the absorption band at 537 nm and the disappearance of the initially existing **3CBD** peak at 430 nm (Fig. 3B). This was accompanied by a significant colour change from yellow to pink (Fig. 4). The selectivity of Hg^{2+} over the other competitive cations is ascribed to the chemistry of the cationic mercury with

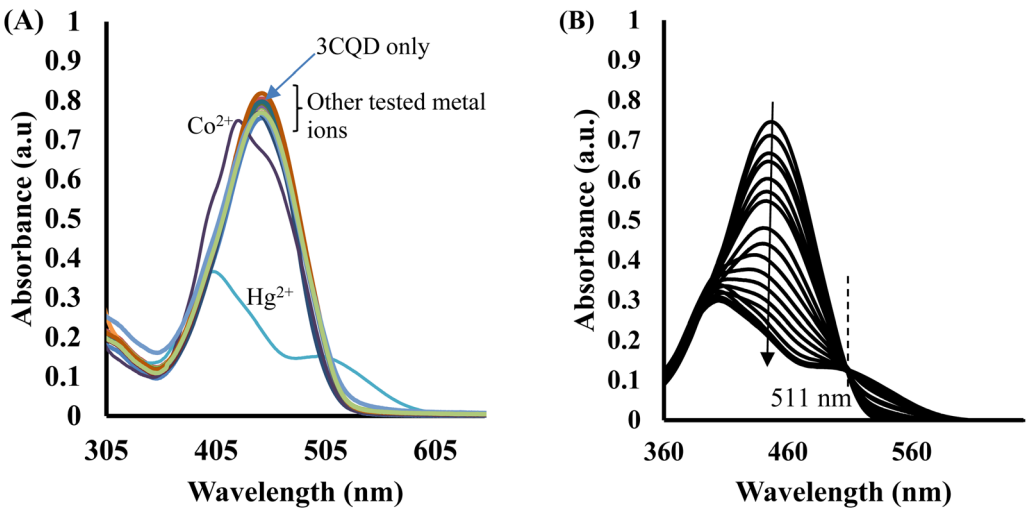

Fig. 1 (A) Absorption spectra changes of **3CQD** (1.56×10^{-4} M) in the presence of 0.5 molar equivalence of different metal ions in water : ethanol (2 : 1); (B) absorption spectra of **3CQD** (1.56×10^{-4} M) in 2 : 1 water : ethanol solution upon stepwise addition of Hg^{2+} 4 molar equivalences.

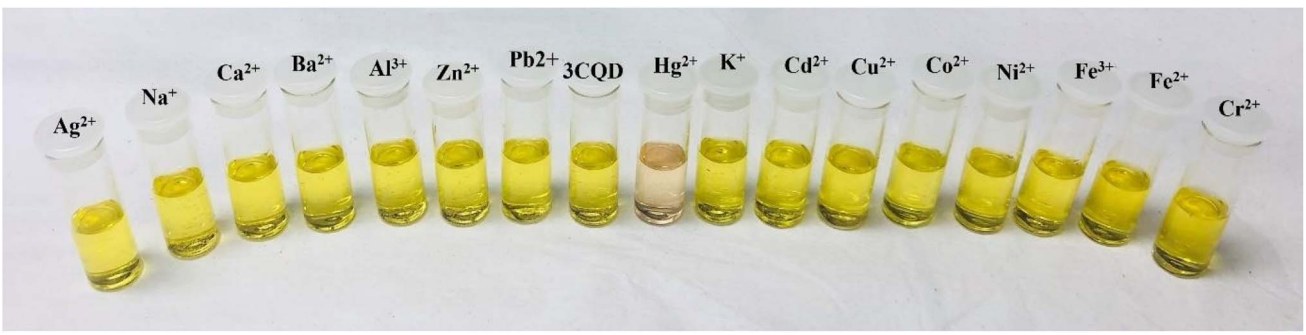

Fig. 2 Colour changes observed in solution of **3CQD** (1.56×10^{-4} M) in the presence of 0.5 equivalence of different metal ions in 2 : 1 water : ethanol solution. Metal ion concentration 0.01 M.

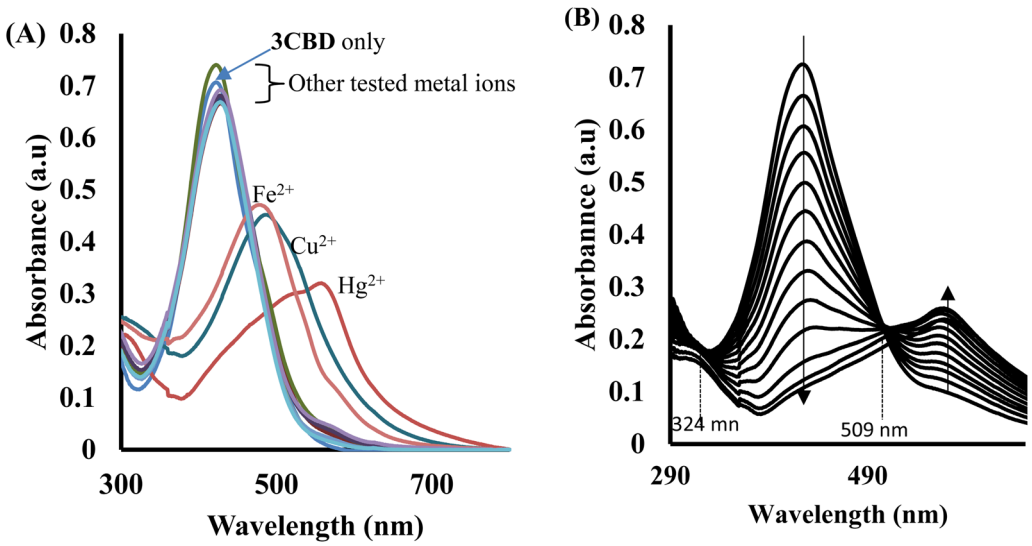

Fig. 3 (A) Absorption spectra changes of **3CBD** (1.58×10^{-4} M) in the presence of 1 molar equivalence of different metal ions in water: acetonitrile; (B) absorption spectra of **3CBD** (1.58×10^{-4} M) in 1 : 1 (water : acetonitrile) upon stepwise addition of 4 molar equivalence of Hg^{2+}.

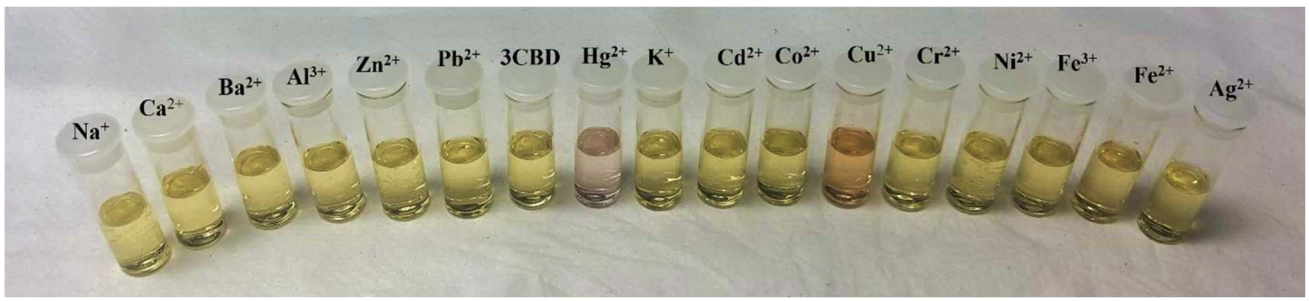

Fig. 4 Colour changes observed in solution of **3CBD** (1.58×10^{-4} M), in the presence of 1 molar equivalence of different metal ions in 1 : 1 water : acetonitrile. Metal ion concentration 0.01 M.

regard to its atomic size, the chemical environment influenced by the solvent used, in relation to the complementary receptors of the ligands, matching the binding/coordinating cavities, which is specific, sensitive and selective only to a particular cation, Hg^{2+} in this case.

3.1.2. Competition studies of 3CBD and 3CQD. To evaluate the selectivity of **3CQD** for Hg^{2+} over other interfering metal

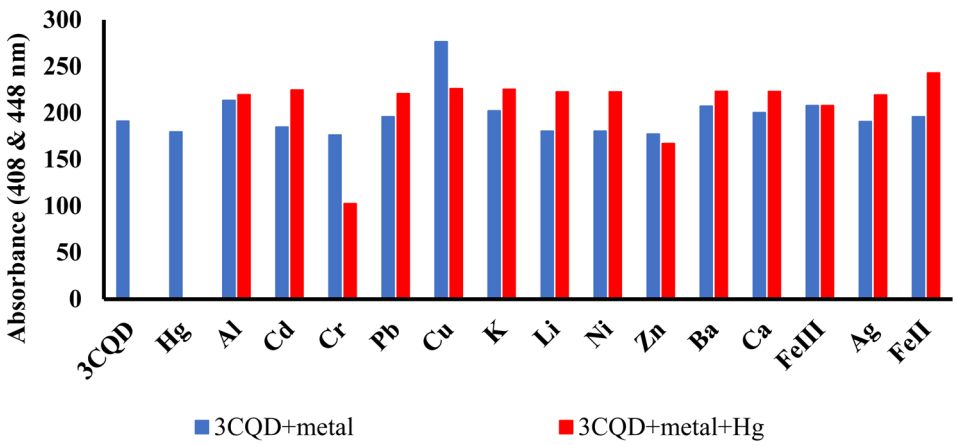

Fig. 5 Absorption responses of **3CQD** (1.56×10^{-4} M) upon addition of 0.5 molar equivalent of various metal ions (red bar) and upon addition of 0.5 molar equivalent of Hg^{2+} with 0.5 molar equivalent other metal ions (blue bars). The experiments were performed in 2 : 1 water : ethanol solution. Metal ion concentration 0.01 M.

cations, competition experiments were conducted. A solution of **3CQD** containing 0.5 molar equivalence of a competing ion was prepared, and then 0.5 molar equivalence of Hg^{2+} was added while monitoring the absorbance. The results, shown in the bar diagram (Fig. 5), indicate that none of the tested metal ions interfered with the detection of Hg^{2+}.

Similar experiments were carried out to assess the selectivity of **3CBD** for Fe^{2+}, Cu^{2+}, and Hg^{2+}. Surprisingly, none of the competing metal ions, including Fe^{2+} and Cu^{2+}, were able to compete with Hg^{2+} (Fig. 6). This suggests that even in the presence of Fe^{2+} or Cu^{2+}, **3CBD** consistently forms a complex with Hg^{2+}, making it a highly selective chemosensor for Hg^{2+}.

3.1.3. Determining binding stoichiometry, association constant, and limit of detection. The binding stoichiometry and association constants (K_s) of the complexes **3CQD**–Hg^{2+} and **3CBD**–Hg^{2+} were determined using the Jobs plot with the continuous variation method[65] and the Benesi–Hildebrand equation. Absorbance was plotted against the molar fraction of Hg^{2+}. The **3CQD**–Hg^{2+} complex exhibited maximum absorbance at a molar fraction of 0.5, indicating a 1 : 1 stoichiometry of complex formation (Fig. 7A). To evaluate the association constants (K_s), the absorbance data were further analyzed. The $1/A_o - A$ values, where A is the absorption intensity in the presence of different concentrations of Hg^{2+} and A_o is the absorption intensity in the absence of Hg^{2+}, were plotted against $1/Hg^{2+}$. The data were fitted linearly to the Benesi–Hildebrand equation, from which the association constants (K_a) were obtained using the slope and intercept of the line (Fig. 7B).

Similarly, the **3CBD**–Hg^{2+} complex exhibited maximum absorbance at a molar fraction of 0.5, indicating a 1 : 1 stoichiometry of complex formation (Fig. 8A), and the association constant for Hg^{2+} binding with **3CBD** was determined to be 7.43 $\times 10^5$ M^{-1} (Fig. 8B). Furthermore, the limits of detection (LOD) and quantification (LOQ) for both probes in detecting Hg^{2+} were determined using the same method. Surprisingly, both probes exhibited similar LOD and LOQ values of 0.03 μM and 0.10 μM, respectively.[66]

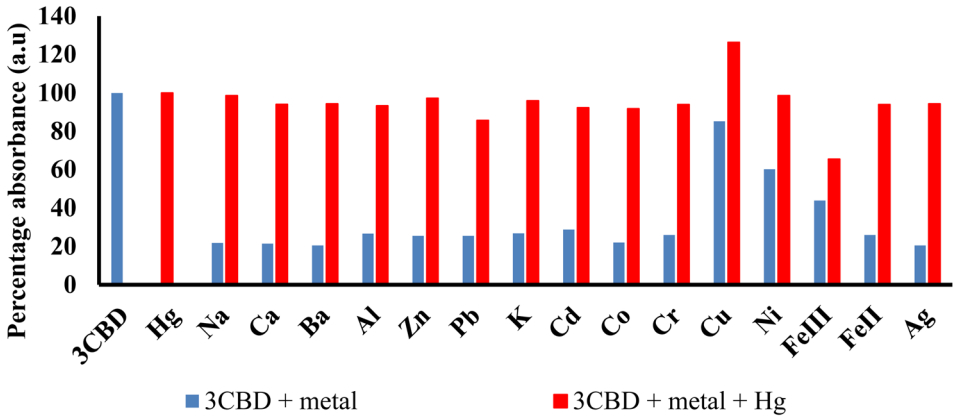

Fig. 6 Absorption responses of **3CBD** (1.58×10^{-4} M) upon addition of 1 molar equivalent of various metal ions (red bar) and upon addition of 1 molar equivalent of Hg^{2+} with 1 molar equivalent other metal ions (blue bars). The experiments were performed in 1 : 1 water : acetonitrile solution. Metal ion stock solutions of 0.01 M.

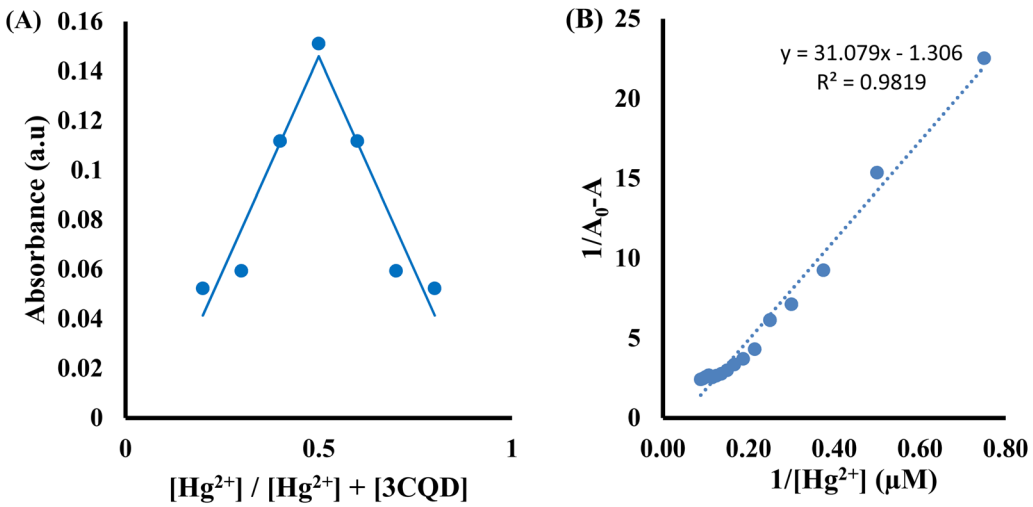

Fig. 7 (A) A Job's plot for **3CQD**–Hg^{2+} binding in 2 : 1 water : ethanol with a constant total concentration of 1.56×10^{-4} M; (B) Benesie–Hildebrand plot of $1/(A_o - A)$ against $1/[Hg^{2+}]$ to calculate the binding constant between **3CQD** and Hg^{2+} and the limit of detection of **3CQD**.

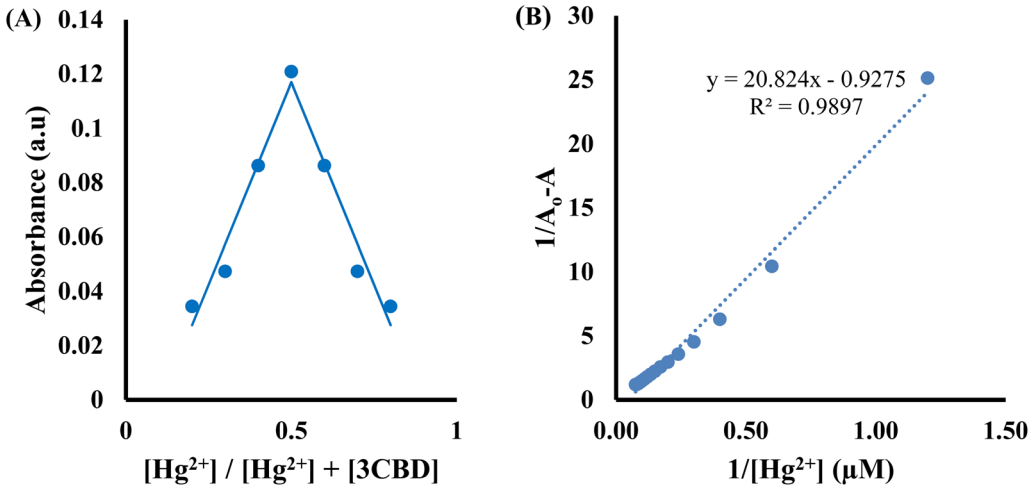

Fig. 8 (A) A Job's plot for 3CBD–Hg^{2+} binding in 1 : 1 water : acetonitrile solution with a constant total concentration of 1.58×10^{-4} M; (B) Benesie–Hildebrand plot of $1/(A_o - A)$ against $1/[Hg^{2+}]$ to calculate the binding constant between 3CBD and Hg^{2+} as well as the limit of detection of 3CBD.

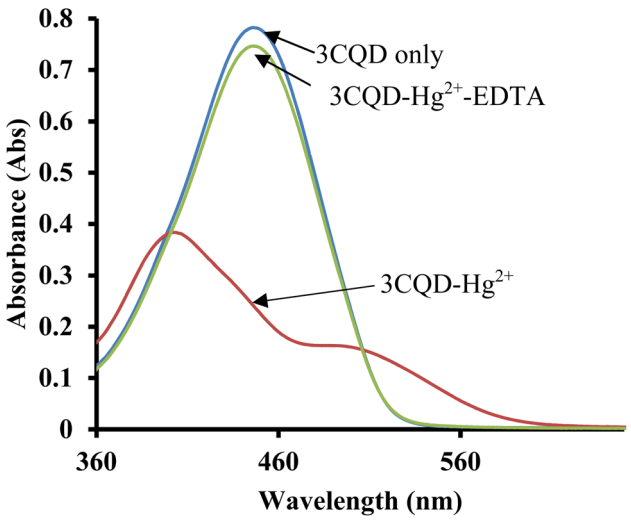

Fig. 9 Reversibility studies of the binding process between 3CQD–Hg^{2+} upon addition of 0.5 molar equivalence of EDTA.

3.1.4. Reversibility studies of 3CQB. The reversibility of the binding mechanisms is a crucial aspect for the practical application of the sensing system, as it enables reusability. Therefore, the reversibility of **3CQD** was examined in the presence of ethylenediaminetetraacetic acid (EDTA), a versatile ligand. Upon the addition of an excess of EDTA to the solution of **3CQD**–Hg^{2+} complex in ethanol: water, the absorbance of the complex reverted back to the original absorbance of **3CQD** (Fig. 9). This observed reversal could be attributed to the dissociation of the carboxylic acid groups of EDTA ligand, which release protons to protonate the lone pair of electrons involved in Hg^{2+} binding.[67]

3.2 Fluorescence assay

In its unbound state, **3CBD** exhibited a maximum emission at 410 nm (λ_{ex} = 340 nm). To demonstrate its potential as a fluorescent chemosensor, a fluorescence titration was performed by adding 3.5 molar equivalence of various cations (Ag^{+}, Na^{+}, Al^{3+}, Ca^{2+}, Ba^{2+}, Fe^{2+}, Fe^{3+}, Cr^{3+}, Hg^{2+}, Cu^{2+}, Co^{2+}, Cd^{2+}, Zn^{2+}, Li^{+}, Pb^{2+}, and Ni^{2+}) to a solution of **3CBD** in ethanol: water at pH 7.0. Among the tested cations, only the addition of Fe^{3+} resulted in a decrease in fluorescence emission (Fig. 10). Interestingly, **3CQD** exhibited low emission intensity in its ground state, indicating the absence of a highly conjugated system due to the delocalization of the lone pair of oxygen in the hydroxyl group attached to the coumarin moiety. None of the tested metal ions were able to activate the intramolecular charge transfer process (ICT) to restore conjugation, which would trigger a "turn-on" response in the emission spectra through chelation-enhanced fluorescence of the molecule.[68]

3.2.1. Fluorescence titration of 3CBD with Fe^{3+}. Fluorescence titration experiments were performed by progressively adding Fe^{3+} ions, which resulted in a gradual decrease in the

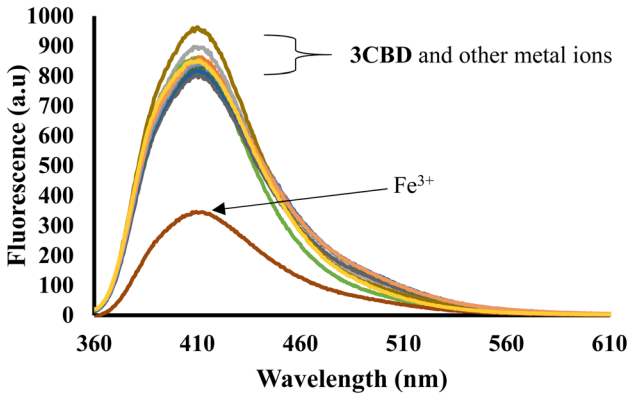

Fig. 10 Emission spectra of 3CBD (1.58×10^{-4} M) in the presence of the aliquot (6.67×10^{-4} M) of different metal ions. The experiments were conducted in ethanol : water solution, excited at 340 nm.

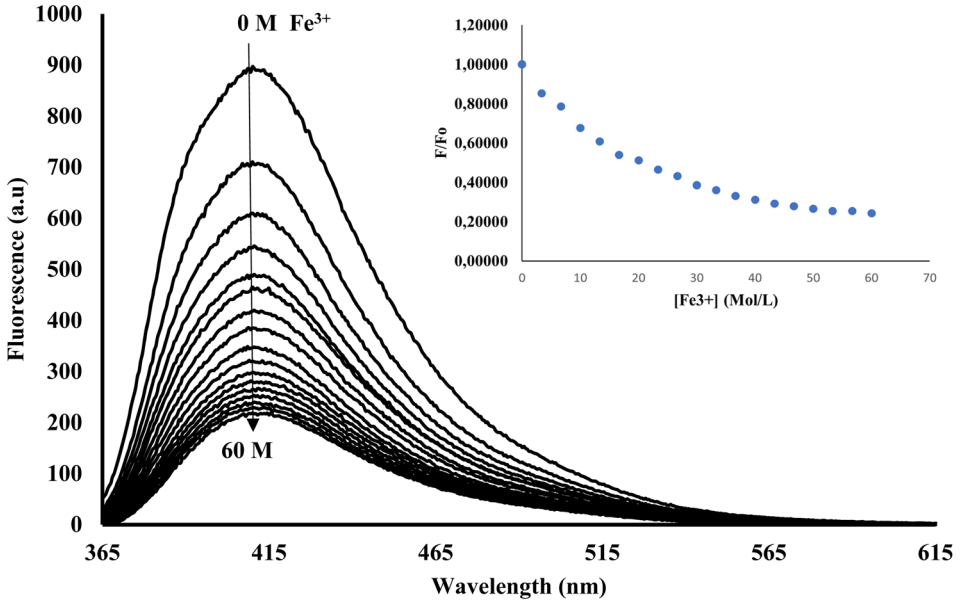

Fig. 11 Emission spectra of **3CBD** (1.58×10^{-4} M) in the presence of the aliquot 60 molar equivalence of different metal ions.

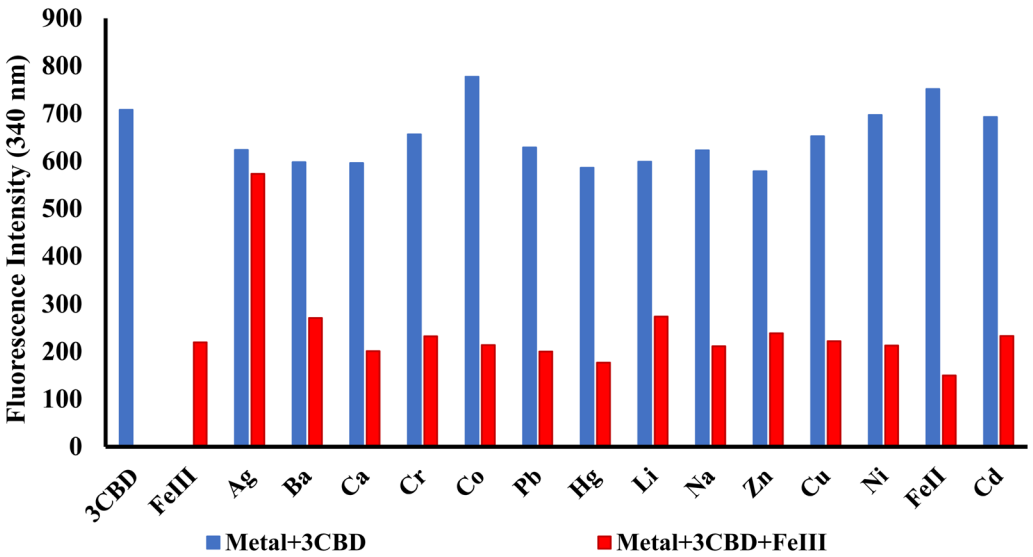

Fig. 12 Fluorescence responses of **3CBD** (1.58×10^{-4} M) upon addition of 127 molar equivalence of various metal ions (blue bar) and upon addition of Fe^{3+} with 127 molar equivalents of other metal ions (red bars) in water: acetonitrile solution. Metal ion stock solutions (0.01 M). Excitation of 340 nm.

emission intensity at 412 nm, as depicted in Fig. 11. Subsequently, the limit of detection, limit of quantification, and the association constants for the binding of Fe^{3+} with **3CBD** were calculated using the Benesi–Hildebrand equation based on the obtained emission intensity results.

3.2.2. Competition studies. The selectivity of **3CBD** towards Fe^{3+} was assessed through competition experiments. In these experiments, 3.5 molar equivalents of various competing metal ions were added to the probe, followed by the addition of an equivalent amount of Fe^{3+}, while monitoring the changes in emission. Among the tested cations (Na^+, Al^{3+}, Ca^{2+}, Ba^{2+}, Fe^{2+}, Fe^{3+}, Cr^{3+}, Hg^{2+}, Cu^{2+}, Co^{2+}, Cd^{2+}, Zn^{2+}, Li^+, Pb^{2+}, and Ni^{2+}, only Ag^+) demonstrated significant interference with the detection of Fe^{3+}, as illustrated in Fig. 12.

3.3 Computation calculations

To gain further insights into the electronic transitions, the structures of the uncomplexed forms (**3CBD** and **3CQD**) as well as the complexed forms (**3CBD**–Hg^{2+} and **3CQD**–Hg^{2+}) of the sensors were calculated in gas phase using molecular mechanics (MMFF) and semi empirical (PM3) methods with Spartan '10 molecular modelling software. The calculations revealed a significant decrease in the energy gap (HOMO–LUMO) from the uncomplexed to the complexed forms, as shown in Table 1. This decrease

Table 1 The summary of HOMO–LUMO orbitals and the energy gaps of **3CBD** and **3CQD** in the absence and presence of and Hg^{2+}

Compound	C=O bond length (Å)	N=N bond length (Å)	C=O (Mulliken charge) (electrostatic charge)	Coumarin-N=N (Mulliken charge) (electrostatic charge)	N=N-R (Mulliken charge) (electrostatic charge)	C=N (Mulliken charge) (electrostatic charge)
3CBD	1.212	1.227	−0.340, −0.525	+0.058, +0.015	+0.004, −0.026	−0.080, −0.385
3CBD–Hg^{2+}	1.264	1.247	−0.365, −0.717	+0.118, −0.046	+0.084, +0.100	+0.081, −0.641
3CQD	1.209	1.232	−0.308, −0.501	+0.040, +0.370	+0.001, −0.295	−0.041, −0.632
3CQD–Hg^{2+}	1.242	1.250	−0.352, −0.827	+0.279, +0.285	+0.133, −0.142	+0.181, −0.660

in the energy gap is consistent with the observed spectral changes of both **3CBD** and **3CQD** upon complexation with Hg^{2+}, indicating a red shift.[69] The energy levels of both the highest occupied molecular orbital (HOMO) and lowest unoccupied molecular orbital (LUMO) decreased upon the addition of Hg^{2+} to **3CBD** and **3CQD**, which is indicative of stable orbital sets (LUMO and HOMO). The substantial reduction in the band gap between HOMO and LUMO of the chemosensors is attributed to the chemosensor-to-metal charge transfer between **3CBD** and Hg^{2+}, as well as **3CQD** and Hg^{2+}. These observations suggest that the complexation of both chemosensors with Hg^{2+} results in the formation of stable complexes.[67]

The chemical interaction between the chemosensors and Hg^{2+} induced structural distortion. For example, in the case of **3CBD**, complexation with Hg^{2+} resulted in lengthening of the carbonyl and azide bonds by 0.052 Å and 0.020 Å, respectively. A similar trend was observed in **3CQD**, with the carbonyl bond length increasing by 0.0033 Å and the azide bond length increasing by 0.018 Å. These changes indicate the interaction of these functional groups with Hg^{2+}. The presence of electron-donating groups such

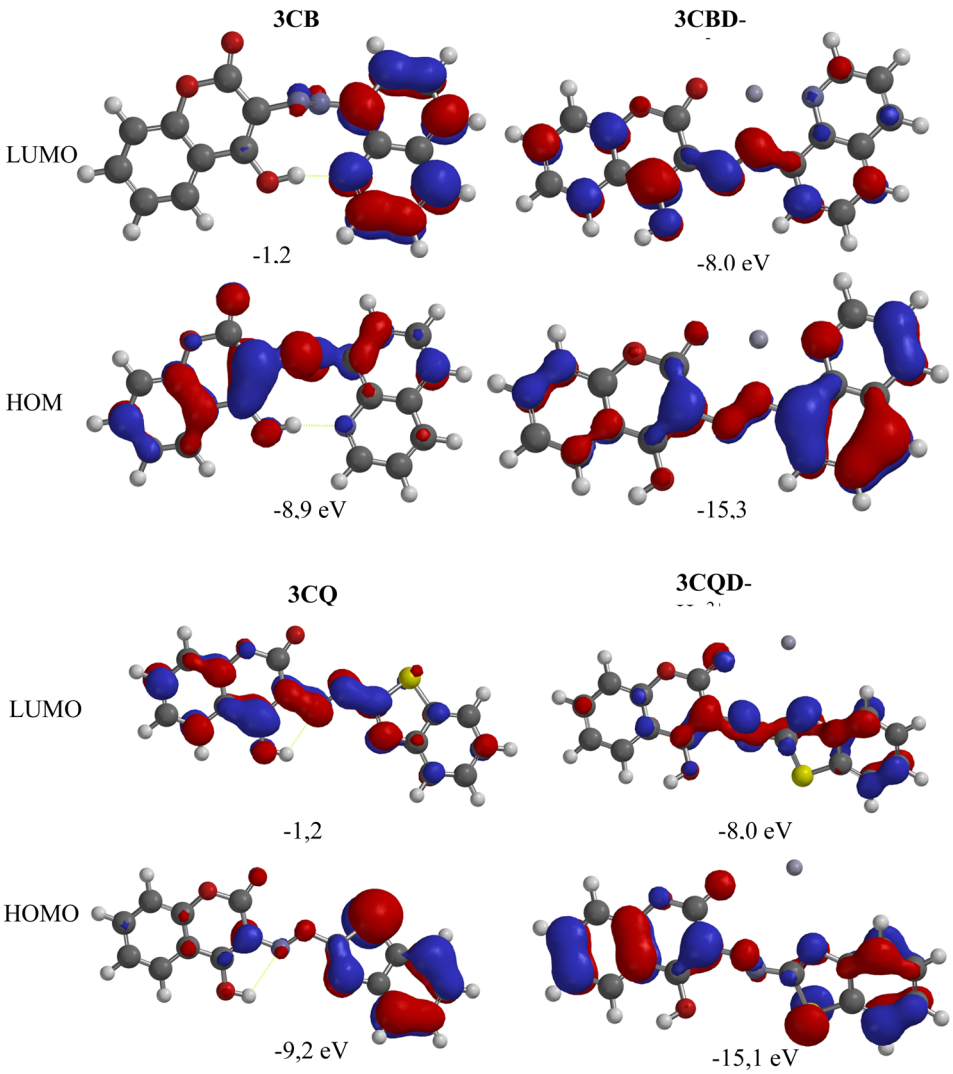

as carbonyls in the complexation with cations affects the stability of the complex. This increased electron-accepting property of the system leads to a reduction in the band gap and consequently a bathochromic effect or a decrease in emission.

3.4 Proposed binding mechanisms

Molecular modelling was utilized to validate the complexation of **3CBD** with Hg^{2+} (Fig. 13A) and **3CQD** with Hg^{2+} (Fig. 13B). The presence of the azo functionality in both compounds

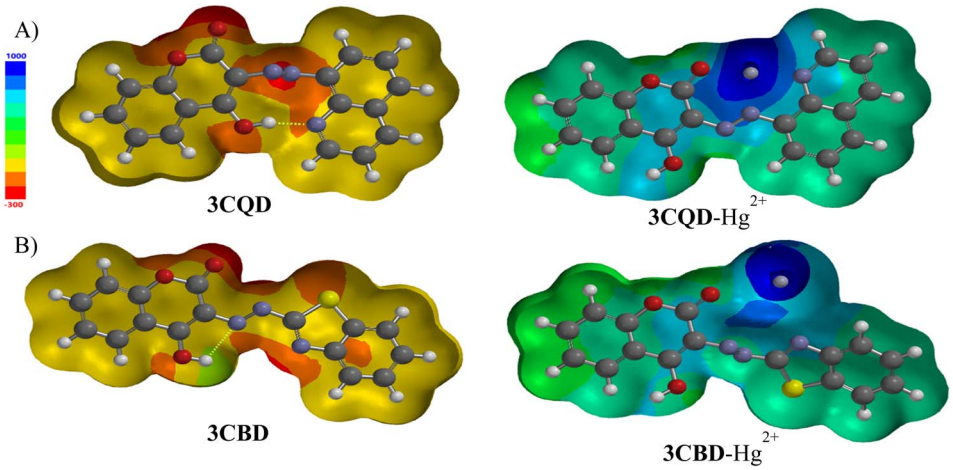

Fig. 13 (A) **3CBD**–Hg^{2+} complex; (B) **3CQD**–Hg^{2+} both at PM3 level using Spartan '10 V1.10.

Table 2 Comparative study on the proposed method and the existing fluorogenic Hg^{2+} probes

Method	LOD	References
3CBD	0.10 μM	Current work
3CQD	0.10 μM	Current work
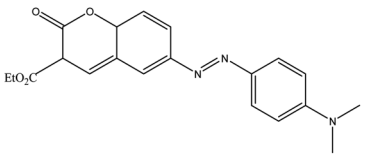	9.45×10^{-3} μM	7
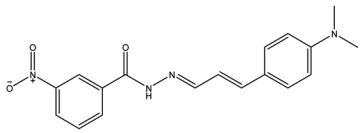	1.1×10^{-1} μM	70
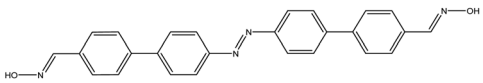	—	71
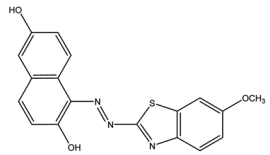	9.45×10^{-3} μM	72
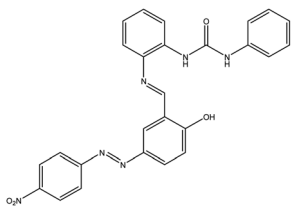	4.89 μM	73
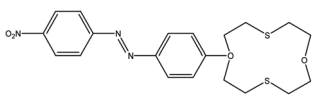	—	74

creates a more electron-dense region that readily accommodates the dication. Upon complexation, it is evident that the rest of the molecule becomes electron-deficient as electrons are drawn towards the Hg^{2+} ion, particularly in the azo region. The hydroxyl group in **3CBD** and the carbonyl group in **3CQD** both contribute to the electron density in the complexation region, facilitating the accommodation of Hg^{2+} (Table 2).

4. Conclusion

In conclusion, the synthesis and characterization of two highly stable and sensitive chemosensors, **3CBD** and **3CQD**, were successfully performed. The sensitivity of these chemosensors towards various cations was evaluated in ACN–H_2O and EtOH–H_2O solutions. Remarkably, both chemosensors exhibited a strong affinity for Hg^{2+} ions, which was confirmed through UV-Vis titration and visual observations of a distinct colour change from yellow to light pink. The binding stoichiometry of the chemosensors with Hg^{2+} was determined to be predominantly 1 : 1 using the job's plot method. The selectivity of the chemosensors relies primarily on charge–charge interactions and the involvement of electron-rich groups such as C=O and N=N in the binding process.

Conflicts of interest

There are no conflicts to declare.

Acknowledgements

This work was supported by the Department of Chemistry, Faculty of Science, Nelson Mandela University, Port Elizabeth, South Africa and Department of Physics, Chemistry and Materials Science, Faculty of Agriculture, Engineering and Natural Sciences, University of Namibia, Windhoek, Namibia.

References

1 F. Chen, F. Hou, L. Huang, J. Cheng, H. Liu, P. Xi, *et al.*, Development of a novel fluorescent probe for copper ion in near aqueous media, *Dyes Pigm.*, 2013, **98**(1), 146–152, DOI: 10.1016/j.dyepig.2013.01.026.

2 H. Sharma, N. Singh and D. Ok, Imidazole and imine coated ZnO nanoparticles for nanomolar detection of Al(III) and Zn(II) in semi-aqueous media, *Tetrahedron Lett.*, 2014, **55**(49), 6623–6626, DOI: 10.1016/j.tetlet.2014.10.080.

3 Y. Keon, U. C. Nam, H. Lim, I. Hong and C. Kim, A selective colorimetric and fluorescent chemosensor based-on naphthol for detection of Al^{3+} and Cu^{2+}, *Dyes Pigm.*, 2013, **99**(1), 6–13, DOI: 10.1016/j.dyepig.2013.04.002.

4 D. Pinheiro, C. S. D. Castro, J. S. Seixas, D. Melo, E. Oliveira, C. Nuñez, *et al.*, From yellow to pink using a fluorimetric and colorimetric pyrene derivative and mercury(II) ions, *Dyes Pigm.*, 2014, **110**, 152–158, DOI: 10.1016/j.dyepig.2014.04.012.

5 H. Y. Lee, X. Song, H. Park, M. H. Baik and D. Lee, Torsionally responsive C3-symmetric azo dyes: azo-hydrazone tautomerism, conformational switching, and application for chemical sensing, *J. Am. Chem. Soc.*, 2010, **132**(34), 12133–12144.

6 O. H. Aremu, C. O. Akintayo, E. B. Naidoo, S. M. Nelana and O. S. Ayanda, Synthesis and applications of nano-sized zinc oxide in wastewater treatment: a review, *Int. J. Environ. Sci. Technol.*, 2021, **18**(10), 3237–3256, DOI: 10.1007/s13762-020-03069-1.

7 A. Battison, S. Schoeman and N. Mama, A coumarin-azo derived colorimetric chemosensor for Hg^{2+} detection in organic and aqueous media and its extended real-world applications, *J. Fluoresc.*, 2023, **33**(1), 267–285.

8 B. Liu, J. Zhuang and G. Wei, Recent advances in the design of colorimetric sensors for environmental monitoring, *Environ. Sci.: Nano*, 2020, **7**(8), 2195–2213.

9 J. G. Speight, Removal of inorganic compounds from the environment, *Environmental Inorganic Chemistry for Engineers*, 2017, 427–478.

10 A. Mohammadi, Z. Dehghan, M. Rassa and N. Chaibakhsh, Colorimetric probes based on bioactive organic dyes for selective sensing of cyanide and fluoride ions, *Sens. Actuators, B*, 2016, **230**, 388–397, DOI: 10.1016/j.snb.2016.02.077.

11 D. S. Powlson and C. J. Dawson, Use of ammonium sulphate as a sulphur fertilizer: implications for ammonia volatilization, *Soil Use Manage.*, 2022, **38**(1), 622–634.

12 X. Shang, X. Li, J. Han, S. Jia, J. Zhang and X. Xu, Colorimetric and fluorescence turn-on sensor for biologically important anions based on carbazole derivative, *Inorg. Chem. Commun.*, 2012, **16**, 37–42, DOI: 10.1016/j.inoche.2011.11.025.

13 Y. Wang, X. Cui, H. Gao, R. Lu and W. Zhou, A fluorescent organic nanoparticles-based sensor synthesized through hydrothermal process and its application in sensing Hg^{2+} of real samples and fast visual detection, *Spectrochim. Acta, Part A*, 2022, **270**, 120833, DOI: 10.1016/j.saa.2021.120833.

14 C. Long, J. H. Hu, Q. Q. Fu and P. W. Ni, A new colorimetric and fluorescent probe based on rhodamine B hydrazone derivatives for cyanide and Cu^{2+} in aqueous media and its application in real life, *Spectrochim. Acta, Part A*, 2019, **219**, 297–306, DOI: 10.1016/j.saa.2019.04.052.

15 X. Tang, X. Zhu, H. Xu, H. Sun, X. Han, Q. Li, *et al.*, Hydrogen-bond activated ESIPT in naphthalimide-based fluorescent probe for sensing volatile amines, *Spectrochim. Acta, Part A*, 2022, **281**, 121567, DOI: 10.1016/j.saa.2022.121567.

16 A. K. Singh, V. K. Gupta and B. Gupta, Chromium(III) selective membrane sensors based on Schiff bases as chelating ionophores, *Anal. Chim. Acta*, 2007, **585**(1), 171–178.

17 E. Hamukwaya, J. Naimhwaka and V. Uahengo, A multi-colorimetric probe to discriminate between heavy metal cations and anions in DMSO-H_2O with high selectivity for Cu^{2+} and CN^-: study of logic functions and its application in real samples, *RSC Adv.*, 2021, **11**(47), 29466–29485.

18 Y. Zhang, Y. Qu, Y. Zhang, Y. Gao and L. Wang, Development of a fluorescent strategy for quantification of fluoride ions in

foods and toothpaste, *Chem. Eng. J.*, 2022, **448**, 137631–137637.

19 Z. G. Ntombela, V. S. R. Pullabhotla and A. K. Basson, Biosafety, Optimization, and Application of Bioflocculant-Synthesized Zinc Oxide Nanoparticles, *Bionanoscience*, 2022, **12**, 1289–1304, DOI: **10.1007/s12668-022-01017-6**.

20 P. B. Tchounwou, C. G. Yedjou, A. K. Patlolla and D. J. Sutton, Molecular, clinical and environmental toxicology volume 3: environmental toxicology, *Molecular, Clinical and Environmental Toxicology*, 2012, **101**, 133–164, DOI: **10.1007/978-3-7643-8340-4**.

21 P. N. Hishimone, E. Hamukwaya and V. Uahengo, The C2-Symmetry Colorimetric Dye Based on a Thiosemicarbazone Derivative and Its Cadmium Complex for Detecting Heavy Metal Cations (Ni^{2+}, Co^{2+}, Cd^{2+}, and Cu^{2+}) Collectively, in DMF, *J. Fluoresc.*, 2021, **31**(4), 999–1008.

22 WHO, *Guidelines for Drinking-Water Quality: Second Addendum*, World Heal Organ Press, 2008, vol. 1, pp. 17–19, **http://www.who.int/water_sanitation_health/dwq/secondaddendum20081119.pdf**.

23 A. Farhan, M. Zulfiqar, S. Samiah, E. U. Rashid, S. Nawaz, H. M. N. Iqbal, *et al.*, Removal of Toxic Metals from Water by Nanocomposites through Advanced Remediation Processes and Photocatalytic Oxidation, *Curr. Pollut. Rep.*, 2023, **9**(3), 338–358, DOI: **10.1007/s40726-023-00253-y**.

24 E. S. Forzani, H. Zhang, W. Chen and N. Tao, Detection of heavy metal ions in drinking water using a high-resolution differential surface plasmon resonance sensor, *Environ. Sci. Technol.*, 2005, **39**, 1257–1262.

25 Y. Zhang, A. Ye, Y. Yao and C. Yao, A Sensitive Near-Infrared Fluorescent Probe for Detecting Heavy Metal Ag^{+} in Water Samples, *Sensors*, 2019, **19**, 247.

26 S. Y. Gwon, B. A. Rao, H. S. Kim, Y. A. Son and S. H. Kim, Novel styrylbenzothiazolium dye-based sensor for mercury, cyanide and hydroxide ions, *Spectrochim. Acta, Part A*, 2015, **144**, 226–234, DOI: **10.1016/j.saa.2015.02.094**.

27 C. Huang and H. Chang, Fluorescent Sensors for Detection of Mercury(II) in ing Hg(II) ions in aqueous solution has been developed in bulk solution fluoresce weakly when they are adsorbed, *Representations*, 2006, **78**(24), 8332–8338.

28 M. Taki, K. Akaoka, S. Iyoshi and Y. Yamamoto, Reversible Detection of a Mercury Ion, *Inorg. Chem.*, 2012, **51**, 13075–13077.

29 X. Cheng, Q. Li, C. Li, J. Qin and Z. Li, Azobenzene-based colorimetric chemosensors for rapid naked-eye detection of mercury(II), *Chem.–Eur. J.*, 2011, **17**(26), 7276–7281.

30 A. Apilux, W. Siangproh, N. Praphairaksit and O. Chailapakul, Simple and rapid colorimetric detection of Hg(II) by a paper-based device using silver nanoplates, *Talanta*, 2012, **97**, 388–394, DOI: **10.1016/j.talanta.2012.04.050**.

31 D. Udhayakumari, Chromogenic and fluorogenic chemosensors for lethal cyanide ion. A comprehensive review of the year 2016, *Sens. Actuators, B*, 2018, **259**, 1022–1057, DOI: **10.1016/j.snb.2017.12.006**.

32 A. K. Singh, S. Mehtab and A. K. Jain, Selective electrochemical sensor for copper(II) ion based on chelating ionophores, *Anal. Chim. Acta*, 2006, **575**(1), 25–31.

33 B. Musikavanhu, S. Muthusamy, D. Zhu, Z. Xue, Q. Yu, C. N. Chiyumba, *et al.*, A simple quinoline-thiophene Schiff base turn-off chemosensor for Hg^{2+} detection: spectroscopy, sensing properties and applications, *Spectrochim. Acta, Part A*, 2022, **264**, 120338, DOI: **10.1016/j.saa.2021.120338**.

34 D. Deng, W. Zhang, X. Chen, F. Liu, J. Zhang, Y. Gu, *et al.*, *Facile Synthesis of High-Quality, Water-Soluble, Near-Infrared-Emitting PbS Quantum Dots*, 2009, pp. 3440–3446.

35 H. Dai and H. Xu, A water-soluble 1,8-naphthalimide-based 'turn on' fluorescent chemosensor for selective and sensitive recognition of mercury ion in water, *Bioorg. Med. Chem. Lett.*, 2011, **21**(18), 5141–5144, DOI: **10.1016/j.bmcl.2011.07.085**.

36 N. I. Georgiev, M. D. Dimitrova, P. V. Krasteva and V. B. Bojinov, A novel water-soluble 1,8-naphthalimide as a fluorescent pH-probe and a molecular logic circuit, *J. Lumin.*, 2017, **187**, 383–391, DOI: **10.1016/j.jlumin.2017.03.049**.

37 Y. Wang, Q. Guo, X. Wu, H. Gao, R. Lu and W. Zhou, A facile and total water-soluble fluorescent organic nanoparticles-based sensor for Hg^{2+} detection and its application in tea samples, *Spectrochim. Acta, Part A*, 2022, **265**, 120358, DOI: **10.1016/j.saa.2021.120358**.

38 E. Hamukwaya, J. Naimhwaka and V. Uahengo, A multi-colorimetric probe to discriminate between heavy metal cations and anions in DMSO-H_2O with high selectivity for Cu^{2+} and CN^{-}: study of logic functions and its application in real samples, *RSC Adv.*, 2021, **11**(47), 29466–29485, DOI: **10.1039/D1RA04734E**.

39 A. Sil, S. N. Islam and S. K. Patra, Terpyridyl appended poly(metaphenylene-alt-fluorene) π-conjugated fluorescent polymers: highly selective and sensitive turn off probes for the detection of Cu^{2+}, *Sens. Actuators, B*, 2018, **254**, 618–628, DOI: **10.1016/j.snb.2017.07.067**.

40 X. Cheng, H. Li, F. Zheng, Q. Lin, Y. Zhang, H. Yao, *et al.*, A pillar[5]arene-based cyanide sensor bearing on a novel cyanide-induced self-assemble mechanism, *Dyes Pigm.*, 2016, **127**, 59–66, DOI: **10.1016/j.dyepig.2015.12.021**.

41 W. L. Guan, Y. F. Zhang, Q. P. Zhang, Y. M. Zhang, T. B. Wei, H. Yao, *et al.*, A novel fluorescent chemosensor based on naphthofuran functionalized naphthalimide for highly selective and sensitive detecting Hg^{2+} and CN^{-}, *J. Lumin.*, 2022, **244**, 118722, DOI: **10.1016/j.jlumin.2021.118722**.

42 M. Theetharappan, L. Subha, C. Balakrishnan and M. A. Neelakantan, Binding interactions of mixed ligand copper(II) amino acid Schiff base complexes with biological targets: spectroscopic evaluation and molecular docking, *Appl. Organomet. Chem.*, 2017, **31**(10), 1–19.

43 B. J. Pages, D. L. Ang, E. P. Wright and J. R. Aldrich-Wright, Metal complex interactions with DNA, *Dalton Trans.*, 2015, **44**(8), 3505–3526, available from: **http://xlink.rsc.org/?DOI=C4DT02700K**.

44 A. Ibezim, M. N. Ofokansi, X. Ndukwe, C. S. Chiama, B. C. Obi, O. N. Isiogugu, *et al.*, Evaluation of anti-malarial potency of new pyrazole-hydrazine coupled to Schiff base derivatives, *Malar. J.*, 2022, **21**(1), 243, DOI: 10.1186/s12936-022-04266-8.

45 T. Kiss, From coordination chemistry to biological chemistry of aluminium, *J. Inorg. Biochem.*, 2013, **128**, 156–163, DOI: 10.1016/j.jinorgbio.2013.06.013.

46 K. S. Min, R. Manivannan and Y. A. Son, Rhodamine-fluorene based dual channel probe for the detection of Hg^{2+} ions and its application in digital printing, *Sens. Actuators, B*, 2018, **261**, 545–552, DOI: 10.1016/j.snb.2018.01.178.

47 J. Isaad and A. El Achari, Water-soluble coumarin based sequential colorimetric and fluorescence on-off chemosensor for copper(II) and cyanide ions in water, *Opt. Mater.*, 2022, **127**, 112275, DOI: 10.1016/j.optmat.2022.112275.

48 F. dos Santos Carlos, M. C. Nunes, L. De Boni, G. S. Machado and F. S. Nunes, A novel fluorene-derivative Schiff-base fluorescent sensor for copper(II) in organic media, *J. Photochem. Photobiol., A*, 2017, **348**, 41–46, DOI: 10.1016/j.jphotochem.2017.08.022.

49 J. H. Naimhwaka, L. Daniel, E. N. Hamukwaya, P. T. Endjala, A. Rahman and V. Uahengo, A Ruthenium Bipyridyl Molecular Dye Sensitizer and an Excited-State Intermolecular Proton Transfer-Active Colorimetric Probe for Anions, with High Affinity Towards CN^- in DMSO, *Chem. Afr.*, 2022, **5**, 19–35, DOI: 10.1007/s42250-021-00299-9.

50 M. W. Wong, H. Xie and S. T. Kwa, Anion recognition by azophenol thiourea-based chromogenic sensors: a combined DFT and molecular dynamics investigation, *J. Mol. Model.*, 2013, **19**(1), 205–213.

51 Y. Peng, Y. M. Dong, M. Dong and Y. W. Wang, A selective, sensitive, colorimetric, and fluorescence probe for relay recognition of fluoride and Cu(II) ions with "off-on-off" switching in ethanol-water solution, *J. Org. Chem.*, 2012, **77**(20), 9072–9080.

52 V. Uahengo, Y. Zhang, B. Xiong, P. Zhao and P. Cai, A Fluoro-Chromogenic Sensor Based on Organic Molecular Framework for Cu^{2+} and F^- in Aqueous Soluble DMSO, *J. Fluoresc.*, 2017, 191–197, DOI: 10.1007/s10895-016-1945-6.

53 S. Pawar, U. Fegade, V. K. Bhardwaj, N. Singh, R. Bendre and A. Kuwar, based fluorescent receptor for dual Ni^{2+} and Cu^{2+} recognition: nanomolar detection, *Polyhedron*, 2015, **87**, 79–85, DOI: 10.1016/j.poly.2014.10.034.

54 S. Tetteh, Coordination Behavior of Ni^{2+}, Cu^{2+}, and Zn^{2+} in Tetrahedral 1-Methylimidazole Complexes: A DFT/CSD Study, *Bioinorg. Chem. Appl.*, 2018, 3157969, DOI: 10.1155/2018/3157969.

55 D. H. Lee, J. H. Im, S. U. Son, Y. K. Chung and J. I. Hong, An azophenol-based chromogenic pyrophosphate sensor in water, *J. Am. Chem. Soc.*, 2003, **125**(26), 7752–7753.

56 M. Orojloo and S. Amani, Naked-eye detection of cyanide ions in aqueous media based on an azo-azomethine chemosensor, *C. R. Chim.*, 2017, **20**(4), 415–423, DOI: 10.1016/j.crci.2016.07.003.

57 S. Suganya and S. Velmathi, Simple azo-based salicylaldimine as colorimetric and fluorescent probe for detecting anions in semi-aqueous medium, *J. Mol. Recognit.*, 2013, **26**(6), 259–267.

58 A. K. Mahapatra, K. Maiti, P. Sahoo and P. K. Nandi, A new colorimetric and fluorescent bis(coumarin)methylene probe for fluoride ion detection based on the proton transfer signaling mode, *J. Lumin.*, 2013, **143**, 349–354, DOI: 10.1016/j.jlumin.2013.05.002.

59 H. A. El-Shekheby, A. H. Mangood, S. M. Hamza, A. S. Al-Kady and E. Z. M. Ebeid, A highly efficient and selective turn-on fluorescent sensor for Hg^{2+}, Ag^+ and Ag nanoparticles based on a coumarin dithioate derivative, *Luminescence*, 2014, **29**(2), 158–167.

60 U. Yanar, B. Babür, D. Pekyilmaz, I. Yahaya, B. Aydiner, Y. Dede, *et al.*, A fluorescent coumarin-thiophene hybrid as a ratiometric chemosensor for anions: synthesis, photophysics, anion sensing and orbital interactions, *J. Mol. Struct.*, 2016, **1108**, 269–277.

61 N. M. Aljamali, Review in Azo Compounds and Its Biological Activity, *Biochem. Anal. Biochem.*, 2015, **04**(02), 2–5.

62 X. Q. Ma, Y. Wang, T. B. Wei, L. H. Qi, X. M. Jiang, J. D. Ding, *et al.*, A novel AIE chemosensor based on quinoline functionalized pillar[5]arene for highly selective and sensitive sequential detection of toxic Hg^{2+} and CN^-, *Dyes Pigm.*, 2019, **164**, 279–286.

63 V. K. Gupta, N. Mergu, L. K. Kumawat and A. K. Singh, Selective naked-eye detection of magnesium(II) ions using a coumarin-derived fluorescent probe, *Sens. Actuators, B*, 2015, **207**, 216–223.

64 M. I. Velasco, C. O. Kinen, R. Hoyos De Rossi and L. I. Rossi, A green alternative to synthetize azo compounds, *Dyes Pigm.*, 2011, **90**(3), 259–264.

65 J. S. Renny, L. L. Tomasevich, E. H. Tallmadge and D. B. Collum, Method of continuous variations: applications of job plots to the study of molecular associations in organometallic chemistry, *Angew. Chem., Int. Ed.*, 2013, **52**(46), 11998–12013.

66 M. Thompson, S. L. R. Ellison, A. Fajgelj, P. Willetts and R. Wood, Harmonised guidelines for the use of recovery information in analytical measurement (technical report), *Pure Appl. Chem.*, 1999, **71**(2), 337–348.

67 J. M. V. Ngororabanga, C. B. Moyo and Z. R. Tshentu, A novel multidentate pyridyl ligand: a turn-on fluorescent chemosensor for Hg^{2+} and its potential application in real sample analysis, *Spectrochim. Acta, Part A*, 2020, **242**, 118651.

68 G. Bartwal, K. Aggarwal and J. M. Khurana, Quinoline-ampyrone functionalized azo dyes as colorimetric and fluorescent enhancement probes for selective aluminium and cobalt ion detection in semi-aqueous media, *J. Photochem. Photobiol., A*, 2020, **394**, 112492.

69 J. Naimhwaka and V. Uahengo, A naphthoquinone based colorimetric probe for real-time naked eye detection of biologically important anions including cyanide ions in tap water: experimental and theoretical studies, *RSC Adv.*, 2019, **9**(65), 37926–37938.

70 A. Kim, S. Kim and C. Kim, A conjugated Schiff base-based chemosensor for selectively detecting mercury ion, *J. Chem. Sci.*, 2020, **132**(1), 1–7.

71 J. Sivamani, V. Sadhasivam and A. Siva, Aldoxime based biphenyl-azo derivative for self-assembly, chemosensor (Hg^{2+}/F^{-}) and bioimaging studies, *Sens. Actuators, B*, 2017, **246**, 108–117.

72 M. D. Gholami, S. Manzhos, P. Sonar, G. A. Ayoko and E. L. Izake, Dual chemosensor for the rapid detection of mercury(II) pollution and biothiols, *Analyst*, 2019, **144**(16), 4908–4916.

73 H. Hosseinjani-Pirdehi, N. O. Mahmoodi, M. Pasandideh Nadamani and A. Taheri, Novel synthesized azo-benzylidene-thiourea as dual naked-eye chemosensor for selective detection of Hg^{2+} and CN^{-} ions, *J. Photochem. Photobiol., A*, 2020, **391**, 112365.

74 Y. Yan, Y. Hu, G. Zhao and X. Kou, A novel azathia-crown ether dye chromogenic chemosensor for the selective detection of mercury(II) ion, *Dyes Pigm.*, 2008, **79**(2), 210–215.